Revision - GRL 07/27/2022

Seasonal Variations of Medium-Scale Waves observed by ICON-MIGHTI

Chihoko Y. Cullens[1,2], Scott England[3], Thomas J. Immel[2], Astrid Maute[4], Brian J. Harding[2], Colin Triplett[2], Jonathan J. Makela[5], Michael H. Stevens[6]

1. Laboratory for Atmospheric and Space Physics, University of Colorado at Boulder
2. Space Sciences Laboratory, University of California Berkeley
3. Virginia Polytechnic Institute and State University
4. High Altitude Observatory, National Center for Atmospheric Research
5. Department of Electrical and Computer Engineering, University of Illinois Urbana-Champaign
6. Space Science Division, Naval Research Laboratory, Washington, DC

Highlight

1. Medium-Scale Perturbations (MSP) are identified in MIGHTI temperature and wind profiles from 90 to 250 km in altitude.
2. MSP show semi-annual variations below ~130 km and annual variations above ~160 km.
3. Seasonal variations of MSP are influenced by background winds and tropospheric sources.

Abstract

This work presents an analysis of seasonal variations of medium-scale perturbations (~500 to ~5700 km) spanning altitudes from 90 km to 250 km using temperature and wind measurements made by the Michelson Interferometer for Global High-resolution Thermospheric Imaging (MIGHTI) instrument onboard the Ionospheric Connection Explorer (ICON) in the latitude range of 0°-40° N during 2020-2021. Both Medium-scale perturbations (MSP) in temperature and winds below ~120 km show semi-annual variations, whereas annual variations of MSP for winds become dominant between 160 km to 250 km. The largest wind MSP was observed at ~110-120 km throughout the year. Spatial variations of MSP at 90-250 km do not show clear geographic patterns in either temperature or wind. Our analysis suggests both seasonal variations of MSP between 90 and 250 km altitudes are influenced by variation on both the sources of MSP and changes in the background wind.

1. Introduction

Gravity waves are small-scale atmospheric waves that distribute momentum and energy from source regions over large geographic distances and altitude and exert significant influence on the dynamics of the atmosphere, from the troposphere to the thermosphere and the ionosphere [e.g., *Fritts and Alexander*, 2003, Vadas and Liu, 2009; Yigit et al., 2009; Miyoshi et al., 2014; Yiğit, 2017; Yiğit and Medvedev, 2017, Becker and Vadas, 2018]. Vadas and Liu [2013] and Liu and Vadas [2013] presented that convectively generated gravity waves propagate to the thermosphere and their wave breaking have significant influences on the ionosphere and the thermosphere using convective model, ray-tracing, and TIME-GCM model. Yigit et al. [e.g., 2009, 2012, 2017] extended GW parametrization up to the thermosphere and presented a strong GW influence on the thermosphere and the ionosphere. Their parametrization results are supported by high-resolution simulations of Miyoshi et al. [2015]. Miyoshi et al. [2015] uses a whole atmospheric model (GAIA model) that resolves GW from the lower atmosphere to the thermosphere (~500 km) and confirmed strong GW drag in the thermosphere. In addition to propagations from the lower atmosphere, secondary/tertiary generation of gravity waves by dissipation of primary gravity waves that are generated in the troposphere and the stratosphere can be an important source in the thermosphere [e.g., Vadas, 2013; Becker & Vadas, 2018]. These previous modeling studies have shown the importance of GWs on the variabilities in the ionosphere and the thermosphere.

Observations of gravity waves in the thermosphere have been reported using GOCE satellite observations [e.g., Forbes et al., 2016; Liu et al., 2017]. Liu et al. [2017] presented annual and semi-annual gravity wave variations with the peak in June-August using GOCE neutral density between 220 to 280 km altitudes (average height is ~250 km). Forbes et al. [2016] showed hemispheric differences and latitudinal variations of GOCE gravity wave density variance. Besides GOCE gravity wave studies, thermospheric global gravity wave observations are rare. In particular, there is a lack of global gravity wave observations between the MLT (the mesosphere and the lower thermosphere) and ~250 km altitude region. Additional observational studies to understand distributions of medium-scale perturbations that includes gravity waves can be beneficial for validations of whole atmospheric models in the thermosphere. Since December 2019, the Michelson Interferometer for Global High-Resolution Thermospheric Imaging (MIGHTI) instrument on the Ionospheric Connection Explorer (ICON) satellite has been providing winds from 90 km to 290 km and temperature measurements from 90 to 127 km in daytime, with a more limited altitude range at night. In this work, using MIGHTI-temperature and winds, perturbations with horizontal scales smaller than ~5000-6000 km are extracted and defined as medium-scale perturbations (MSP), which include gravity wave perturbations. Results of temporal, spatial, and altitudinal variations of medium-scale wave variances are shown and discussed in this work and provide new insight into medium-scale perturbation variation in the mesosphere and the thermosphere.

2. ICON-MIGHTI and Analysis Method

The Ionospheric Connection Explorer (ICON) was launched October 10, 2019 [*Immel et al.*, 2018]. Temperatures and winds in the upper atmosphere have been measured by the Michelson Interferometer for Global High-Resolution Thermospheric Imaging (MIGHTI) instrument [*Immel et al.*, 2018; *Englert et al.* 2017; *Harlander et al.*, 2017; *Harding et al.*, 2017; Stevens et al., 2018]. In this study, MIGHTI-A temperatures (version 5) from 90 km to 127 km, MIGHTI Greenline winds (version 4) from ~95 km to 150 km and MIGHTI Redline winds (version 4) from 160 km to 250 km are used. Data are continuous through these altitude ranges only in daytime so we focus on the 10 to 16 hour local time range (LT hereafter). The vertical sampling of MIGHTI temperature vertical resolution is ~3 km. The vertical sampling frequency of MIGHTI green-line wind is also ~3 km, and is ~ 10 km for red-line wind. MIGHTI redline winds and greenline winds have been validated against ground based FPI and radar observations, respectively [Makela *et al*., 2021 Harding *et al*., 2021]. Validations of version 4 MIGHTI temperature against ground-based lidar observations can be found in Yuan *et al*. [2021].

Characteristics of MSP are determined from these data by first subtracting background and large-scale waves from the observations. This method is widely used for gravity wave analysis using various satellite observations including SABER, COSMIC, and HIRDLS [e.g., Ern *et* *al.,*2011; Preusse *et al*., 2009; Yamashita *et al*., 2013; Cullens *et al*., 2015]. The analysis method is briefly summarized in the following. For each day of data, MIGHTI winds and temperature data are binned/averaged into 30-minute LT samples. Background and large-scale waves are then estimated by fitting wavenumber 0 to 6 at fixed LT. By fitting wavenumber 0-6 at fixed LT, both zonal-mean backgrounds, tides, and stationary planetary waves are included, even though none of these components can be specifically identified. Estimated background temperature and wind are subtracted from each temperature and wind profile. Residuals (i.e., the difference between the data and the large-scale wave fit) are analyzed to characterize the remaining medium-scale perturbations (MSP), which includes gravity wave perturbations. MSP shown in this work characterize waves with horizontal wavelengths longer than ~500 km and smaller than ~4300-5700 km. The analysis is conducted using data from 0° - 40° N because of large numbers of missing data points due to South Atlantic Anomaly (SAA) that cause zonal coverage to be incomplete in the southern hemisphere and therefore difficult to fit for large-scale waves.

Figure 1 shows an example of MSP analysis. Figure 1a, 1c, and 1e show MIGHTI wind and temperature observations (black dots) and estimated background (combined wavenumber 0-6). Differences between estimated background (redline) and original measurements (black dots) are considered to be medium-scale perturbations in this work. Figures 1b, 1d, and 1f show vertical profiles of MSP with wave-like perturbations for (b,d) zonal wind and (f) temperature. Red dashed lines indicate uncertainties for wind measurements in Figure 1b and 1d and temperature measurements in Figure 1f.

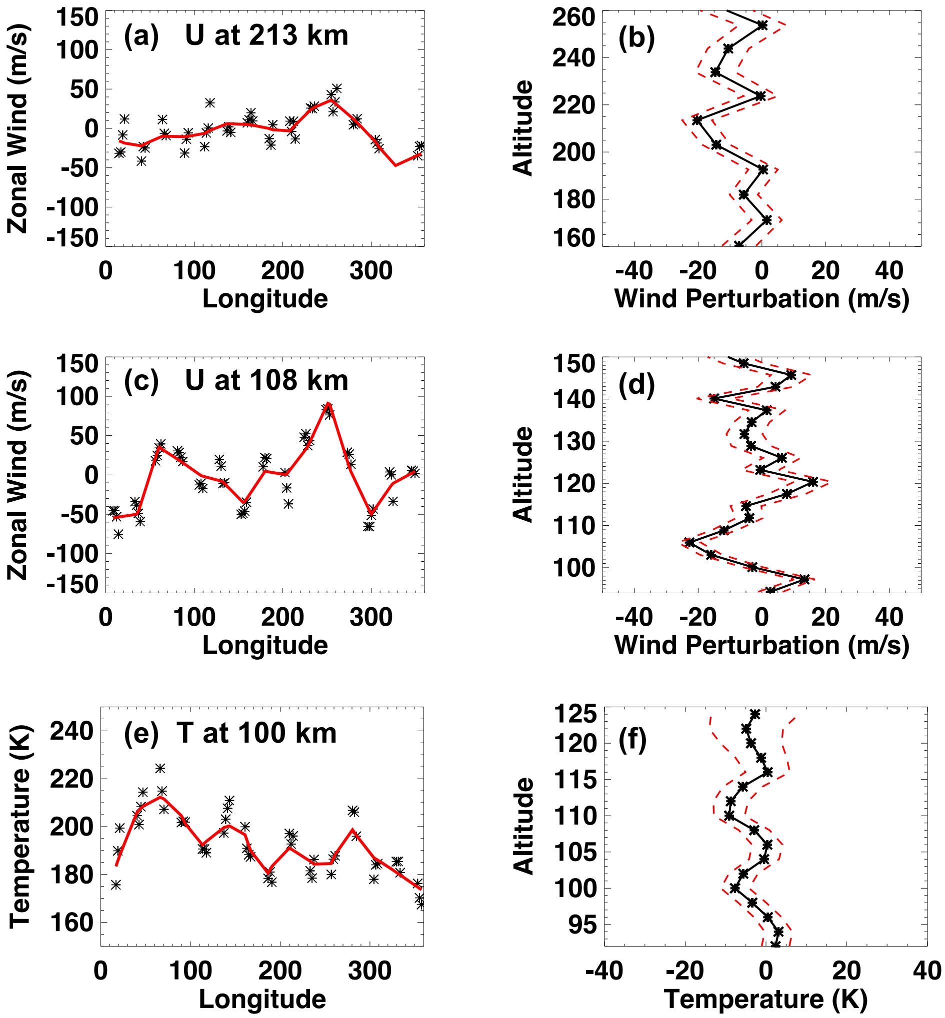

Figure 1. The red line indicates the background zonal winds (wavenumber 0-6) and the black dots indicate MIGHTI measurements for (a, c) the zonal winds measurements at 213 km and at 108 km, respectively, and (e) temperature measurements at 100 km at 14 LT. The vertical profiles of medium-scale perturbations for (b) red line zonal winds, (d) green line zonal winds, and (f) temperature are shown in black lines, and red dotted lines indicate uncertainties of wind and temperature measurements.

3. Results

3.1. Climatology of Medium-Scale Perturbations

Figure 2 shows the seasonal and latitudinal variations of MSP. The wind MSP variances at 200 km and 110 km are depicted in Figures 2a and 2c, respectively, and temperature MSP at 110 km and 94 km are illustrated in Figures 2b and 2d, respectively. MSPs are separated into different latitude ranges of 0-15°N, 15-30°N, and 30-40°N. MSP at 200 km in Figure 2a have the largest variance in June-July at all latitude range (0°-15°N, 15°-30°N, and 30°-40°N). There are secondary peaks in December- January. Peaks MSP variance at 200 km at 15°-30°N and 30°-40°N in June and July are 85-95.0 m^2/s^2 and secondary peak in December and January are ~60 m^2/s^2. The June and July peaks are ~17-26% larger than MSP in December and January in the latitude range of 15°-30°N and 30°-40°N. In the latitude range of 0°-15°N, MSP in June-July are weaker and result in weaker annual variations but larger semi-annual variations (in particular for 2021 results). Minimum MSP for the latitude range of 0°-15°N in March-April and September-October are ~30 - 40 m^2/s^2, which is ~40-50% lower than the peaks in June-July. Although there are MSP peaks in December – January, the annual-variations of MSP is generally dominant at 200 km.

In contrast to MSP variances at 200 km, MSPs at 110 km at all latitudes indicate a dominant semi-annual variation at the two peaks in December-January and June-August. For the latitude range of 15°-30°N, the peak variance in July is ~250-270 m^2/s^2 and December-January peak is ~250 m^2/s^2. Semi-annual variations are largest at 15°-30°N. Minimum MSP in Septembers in the year of 2020 and 2021 are ~180 m^2/s^2 compared to maximum ~260 m^2/s^2 in June-July at 15°-30°N. For the latitude range of 0°-15°N, both July and January peaks are ~200 – 250 m^2/s^2. Forbes et al. [2015] showed GOCE gravity wave variations in the altitude range of ~220 to 280 km. Their results also show the largest peak in June-July and dominate annual variations along with secondary peak in December-January in low latitudes. Our seasonal variations are comparable to previous work at ~250 km.

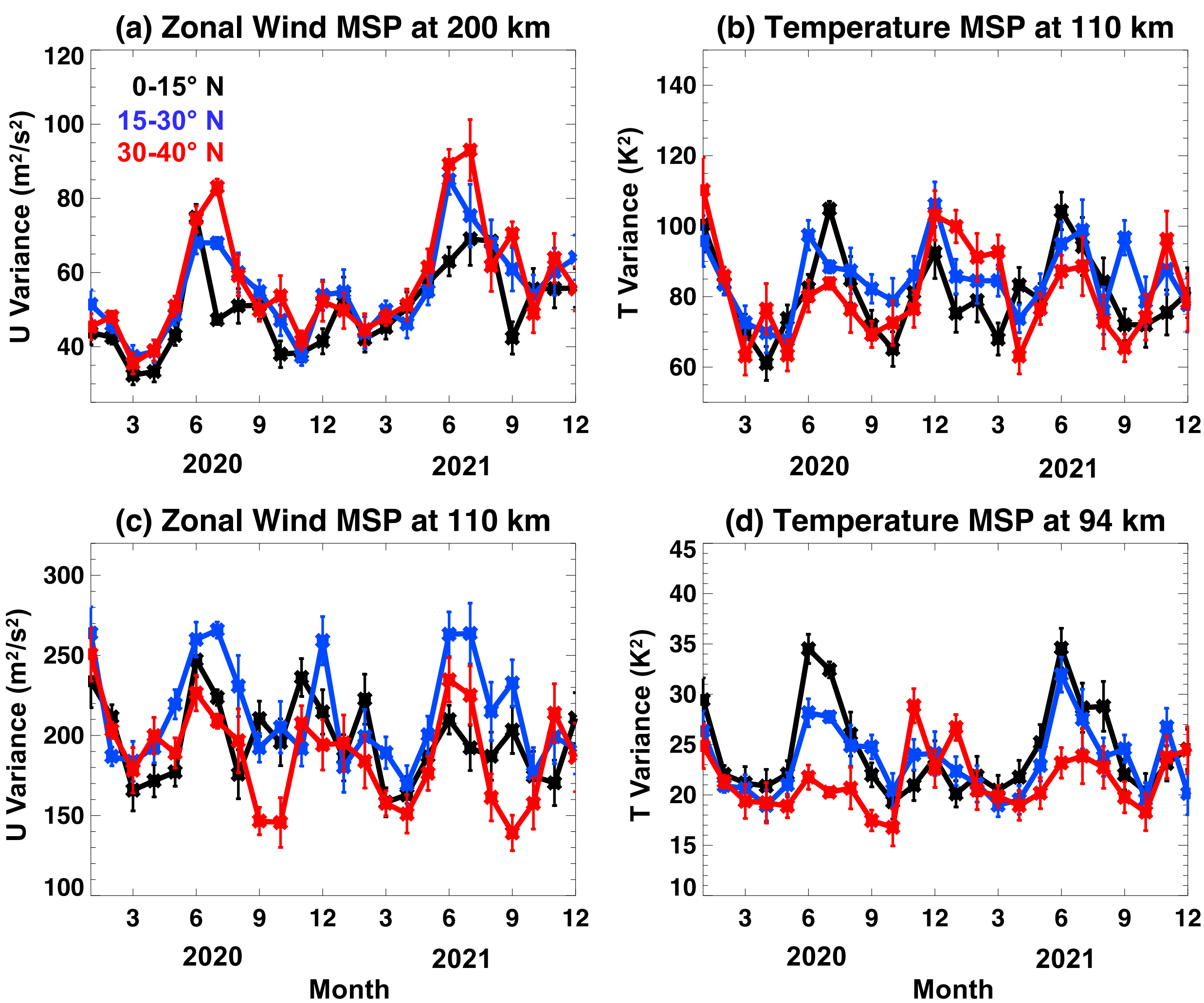

Figure 2. Seasonal variations of monthly-zonal-mean MSP *variances in (a) zonal-winds at 200 km, (b) temperature at 110 km, (c) zonal winds at 110 km, (d) temperature at 94 km averaged over (black) 0-15°N, (blue) 15-30°N, (red) 30-40°N from January 2020 to December 2021. Error bars represent one sigma.*

Temperature MSP variances at 110 km also show a clear semi-annual variation in all the latitude range with peaks in June-July and November-February in Figure 2b. Peak MSP variances in June-July and November-February are ~100-120 K^2 and minimum MSP in March and September are ~60-70 K^2. MSP variance in solstice is ~30-40% larger than those in equinox. At 94 km in Figure 2d, temperature MSP variances at 15°-30°N and 30°-40°N both show semi-annual variations with peaks in June-July and December-January as wind MSP variances. Interestingly, MSPs at 94 km show a dominate annual variation in the latitude range of 0°-15°N, which is different variations from other latitudes. Gravity wave measurements from SABER temperature observations at 95 km also found semi-annual variations with two peaks around June-August and December-January averaged over 12°S - 12°N and from 2002 to 2006 [Preusse *et al.*, 2009]. A cause of differences in seasonal variations between MIGHTI and SABER could be due to the difference in LT coverage. Preusse *et al.* [2009] showed SABER observations covering all LT, but in this study MIGHTI observations in Figure 2 focus only on 10-16 LT to cover wide altitude range (night time temperature observations only go up to 105 km). When we include all local time for MIGHTI below 105 km and recalculate temperature MSP, a semi-annual variation begins to show (Figure not shown). In addition, SABER (5-year average) and MIGHTI (2 years of analysis) observational periods are different. Further comparison between two datasets will be conducted in the future work.

To further study altitudinal variations of MSPs, Figure 3 shows the height variation of the monthly mean MSP variance from January 2020 to December 2021. MSP variances are averaged over 0°-40°N, which include all MSP shown in Figure 2. Figures 3a and 3b show seasonal variations of MSP from MIGHTI winds. Wind MSPs are separated in Figure 3a and 3b to indicate winds derived from red-line and green-line emission, respectively. The MSP variances (94 – 150 km altitudes) in Figure 3b show clear semi-annual variations with peaks in December-January and June-August around solstice. MSP variance at 110-120 km exhibits the largest amplitudes. MSP in June-July in 2021 are weaker than those in 2020 in Figure 3b about ~5-10%.

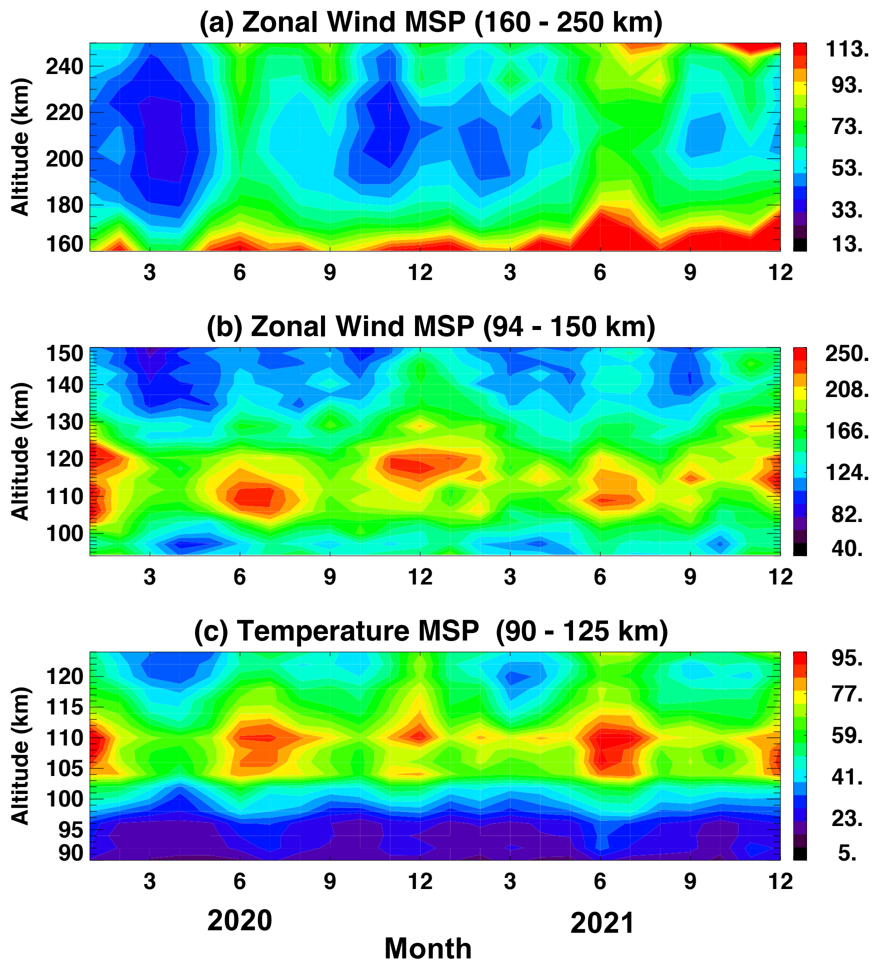

Figure 3. Seasonal variations of monthly-mean MSP *variances from (a) MIGHTI red-line zonal winds* (m^2/s^2)*, (b) MIGHTI green-line zonal winds* (m^2/s^2)*, (c) MIGHTI temperature* (K^2) *averaged over 0°-40°N. The vertical black line marks the end of 2020.*

Figure 3a shows MSP variances from 160 km to 250 km. As shown in Figure 2a, MSP above 180 km have strong annual variations with a peak in June-July. These peaks are evident in both 2020 and 2021. From 160 km to 250 km, MSP amplitudes are decreasing with altitude, which may indicate dissipation of gravity waves propagating from the lower atmosphere [Fritts and Alexander, 2003]. Figure 3c shows temperature MSP variations from 90 km to 125 km. Semi-annual variations are dominated and temperature MSPs maximize between ~105 km and 120 km altitudes, which is consistent with wind MSP observations shown in Figure 3b.

Longitudinal variations of temperature and wind MSP are examined; however, there is no clear longitudinal variations of MSP amplitudes in all altitudes. Miyoshi et al. [2014] presented resolved gravity waves in whole atmospheric models. Their results indicate strong connections of gravity wave in the troposphere to gravity waves in the thermosphere around the region of Andes Mountains but not as clear in the low latitude [Miyoshi et al., 2014]. MIGHTI only observes in the latitude range of 10°S-40°N and does not include Andes Mountain area. GOCE satellite results also did not find a geographically located source of strong gravity wave activities, though GOCE found significant latitudinal variations [Forbes et al., 2016]. Preusse *et al.* [2009] used ray-tracing of gravity waves to explain SABER gravity wave variations at ~95 km. Their results indicate that longitudinal variations of gravity waves in the lower atmosphere disappear as they propagate to 95 km because gravity waves spread out as they propagate upward. At MIGHTI observed altitudes (90-250 km), spatial variations of monthly mean gravity waves seem not to be strongly tied to tropospheric source distributions, which is consistent with previous satellite gravity wave observations.

4. Discussion

In this section, the conditions of sources and propagation of gravity waves will be discussed to explain our observed MSP variations. Figure 4a shows MIGHTI zonal and monthly mean zonal winds from 94 km to 280 km averaged over 10 to 16 LT as in the analyses of Section 3. Zonal mean winds at the altitude range of ~110-150 km show clear annual variations with strong westward winds from May to September. The zonal winds above ~160 km are westward winds throughout the year with largest westward winds in May-August. In order to understand gravity wave propagations below ~95 km, zonal winds from Specified Dynamics Whole Atmosphere Community Climate Model with thermosphere and ionosphere extension (SD-WACCMX) are used in this study and shown in Figure 4b. SD-WACCMX is nudged by GEOS5 below ~60 km to simulate a realistic lower atmosphere [e.g., Kunz *et al*. 2011; Smith *et al*., 2017]. To validate SD-WACCMX zonal wind above 94 km against MIGHTI zonal wind, SD-WACCM-X data is also averaged over 10 LT to 16 LT and in the latitude range of 0°-40°N. Coincident MIGHTI wind altitudes are indicated by a red box in Figure 4b. Between ~90 km to ~125 km, SD-WACCM-X show eastward winds consistently through the year. Although MIGHTI shows westward winds around August and October-November, MIGHTI show no clear seasonal variations with mostly eastward winds from 95 km to ~115 km as similar to SD-WACCM-X. Between 125 km and 300 km, SD-WACCM-X show annual variations with westward from May to August and eastward/weak westward winds from September to ~March. On the other hand, MIGHTI zonal winds are westward through the year between 160 and 280 km. Differences between measured winds and SD-WACCM-X could be due to the lack of gravity wave drag in these heights in SD-WACCM-X. Because MIGHTI zonal wind only includes daytime data, differences between MIGHTI and SD-WACCMX could also be coming from differences in tidal amplitudes and/or phases. Although seasonal variations are not consistent between SD-WACCM-X and MIGHTI from ~160 km to 250 km, magnitudes of the zonal winds in July-August are ~60-70 m/s and consistent between SD-WACCM-X and MIGHTI.

Preusse et al. [2009] show latitudinal variations of gravity waves using SABER observations and a ray-tracing model from 30 km to 90 km. They showed that gravity waves in the tropics in the troposphere and stratosphere spread out to wide range of latitudes range as they propagate upward to the mesosphere and the lower thermosphere. Therefore, MIGHTI MSP in the latitude range of 0°-40°N at the MLT region could be coming from convective region (20°S-20°N) in the lower atmosphere. To understand wave propagations, Figure 4c shows zonal mean zonal wind from 10 km to 100 km from SD-WACCMX averaged over the tropics (latitude range of 20°S-20°N). Zonal winds in Figure 4c are daily mean results including all local time. SD-WACCMX zonal winds show clear semi-annual variations, which is consistent with previous studies of semi-annual oscillations (SAO) [e.g., Garcia et al., 1997; Smith et al., 2017]. The periods of westward phases of SAO in WACCM are shorter than those in HRDI observations [Garcia *et al.*, 1997]; however, the general structures of SAO in WACCMX are compared well with Garcia *et al*. [1997]. Such semi-annual variations in zonal wind structure can be a cause of observed semi-annul variations of gravity waves in the mesosphere and thermosphere as also discussed by previous studies [e.g., Preusse *et al*., 2009] and could affect our observed MSP.

Furthermore, according to both MIGHTI and SD-WACCM-X in Figures 4a and 4b, the zonal wind direction changes from eastward to westward in the altitude range of 130-160 km. Changes in wind direction are often associated with dissipations of gravity waves [Fritts and Alexander, 2003], and such wave dissipation can generate secondary generation of gravity waves [e.g., Vadas 2013]. Wind MSP variance in Figures 3a and 3b show changes from semi-annual variations below 150 km to annual variations above 160 km. The altitude of MSP changes (130-180 km) coincide with changes of zonal wind directions seen both in MIGHTI and SD-WACCMX.

Our results suggest that background wind structure have an important role in observed MSP seasonal variations.

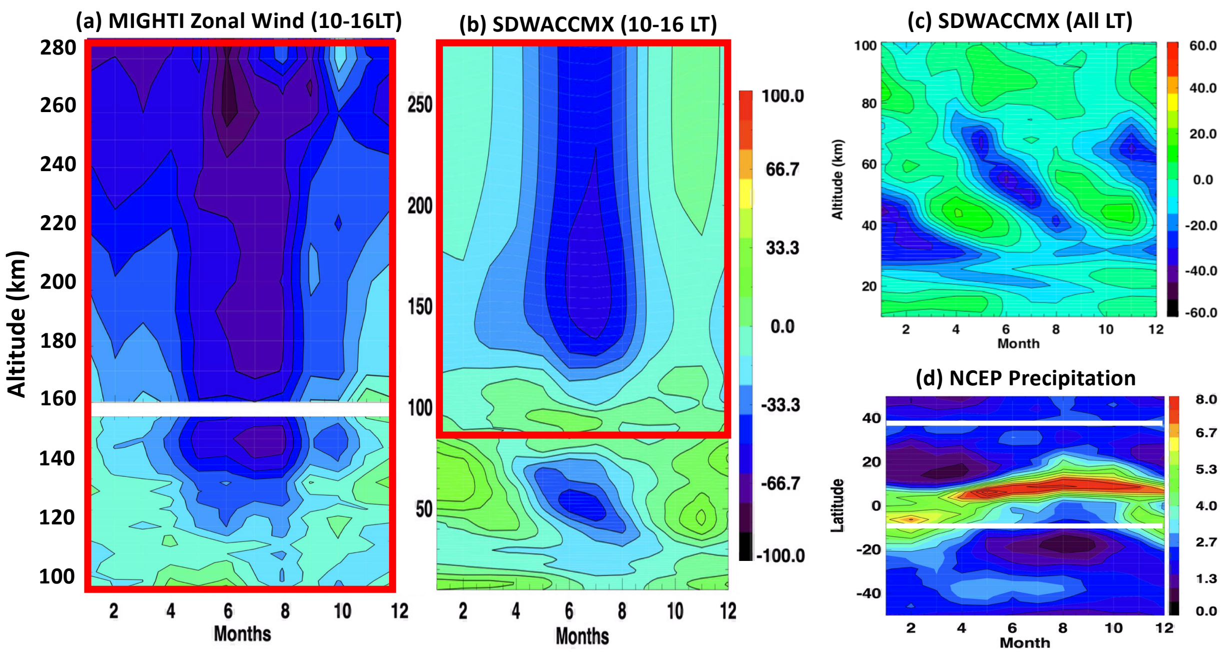

Figure 4. Seasonal variations of (a) MIGHTI zonal-mean zonal winds from 95-280 km and (b) SD-WACCMX zonal mean zonal wind from 10-280 km. Zonal winds in Figure 4a and 4b are averaged over 10-16 LT and latitude range of 0°-40°N. Positive/negative indicate eastward/westward zonal winds, respectively. Red boxes indicate MIGHTI observational altitude. (c) SD-WACCMX zonal and daily (all LT) mean zonal wind in the latitude range of 20S-20N. (d) NCEP monthly mean precipitation in 2020 (mm/day).

We further investigate the connection to gravity wave source variations in the troposphere. Major sources of gravity waves are orography, frontal system, and convection. One of the largest gravity wave sources in the low-latitude troposphere is convection [Fritts and Alexander, 2003].

In order to quantify changes in convective activities, Figure 4d shows NCEP monthly mean zonal mean precipitation obtained for the year of 2020. White lines in Figure 4d show the ICON observational latitudes from 10°S to 40°N. The largest peak in precipitations is in June-September in the latitude range of 0°-20°N. The second peak is in January in the latitude range of 0°-20°S. These two peaks coincident with MIGHTI MSP semi-annual peaks below 150 km in Figures 3b and 3c. Therefore, our observed MIGHTI MSP can be influenced by both semi-annual variations of convective sources in the low latitudes and also zonal wind structures, which consistent with previous studies in the mesosphere region.

Furthermore, geomagnetic activity can also be a source for small to medium scale waves. Bruinsma and Forbes [2008] presented the influences of geomagnetic activity (Kp > 4.5) on small-medium scale waves (600-2400 km) in relative neutral density from high-latitudes to low-latitudes. Although it is possible that geomagnetic activities can affect our observed MSP, there are not many strong geomagnetic activity during our observed time. Influences of geomagnetic activities on medium-scale waves are important and will be further investigated in the following studies.

5. Conclusions

This work presents the first seasonal variations of meidum-scale perturbations from 90 km to 250 km using both temperature and winds in the latitude range of 0°-40°N from January 2020 to December 2021. The MIGHTI instrument onboard the ICON has been providing zonal and meridional winds from 94 km to 280 km and temperature measurements from 90 to 127 km during daytime since December 2019. Medium-scale perturbations (wavelengths between ~500 km and ~5700 km) are extracted from MIGHTI temperature and wind profiles. MSP amplitudes in temperature and winds in the altitude range of ~100-130 km shows clear semi-annual variations, and annual variations of MSP become dominant between 180 km to 250 km. Largest MSP variances are observed at ~110-120 km altitude throughout the year from both winds and temperature. Spatial variations of MSP do not present clear and consistent longitudinal structure in the altitude range of 90-250 km and in the ICON observational range of 0°-40°N in both temperature and winds. This is likely due to changes in background winds below 95 km and that gravity waves originating in the lower atmosphere spread out as they propagate. Our analysis of zonal winds and precipitation data suggests both gravity wave sources and background wind changes can affect seasonal variations of MSP from 90 to 250 km.

Acknowledgement

ICON is supported by NASA's Explorers Program through contracts NNG12FA45C and NNG12FA42I. AM is supported by NASA grant 80NSSC2. CYC is supported by NASA grant 80NSSC22K0726 and NSF 2217461. We would like to acknowledge high-performance computing support from Cheyenne (doi:10.5065/D6RX99HX) provided by NCAR's Computational and Information Systems Laboratory, sponsored by the National Science Foundation. The National Center for Atmospheric Research is sponsored by the National Science Foundation.

Open Research

Data Availability Statement

This analysis used version 04 of the Level 2 ICON MIGHTI wind data and version 05 of the ICON MIGHTI temperature data which are available from the ICON website (https://icon.ssl.berkeley.edu/Data) and NASA's Space Physics Data Facility (https://cdaweb.gsfc.nasa.gov/pub/data/icon/). SD-WACCMX is available from https://doi.org/10.5065/rjgt-g951 [Maute, 2022]. NCEP precipitation data is available at https://psl.noaa.gov/data/gridded/data.cmap.html [Huffman et al., 1997].

Reference

Becker, E., & Vadas, S. L. (2018). Secondary gravity waves in the winter mesosphere: Results from a high-resolution global circulation model. Journal of Geophysical Research: Atmospheres, 123, 2605– 2627. https://doi.org/10.1002/2017JD027460.

Bruinsma, S. L., and Forbes, J. M. (2008), Medium- to large-scale density variability as observed by CHAMP, Space Weather, 6, S08002, doi:10.1029/2008SW000411.

Cullens, C. Y., S. L. England, T. J. Immel (2015), Global responses of gravity waves to planetary wave activities, Journal of Geophysical Research – Atmosphere, 120, 12,018–12,026, doi:10.1002/2015JD023966.

Englert, C.R., J.M. Harlander, C.M. Brown, K.D. Marr, I.J. Miller, J.E. Stump, J. Hancock, J.Q. Peterson, J. Kumler, W.H. Morrow, T.A. Mooney, S. Ellis, S.B. Mende, S.E. Harris, M.H. Stevens, J.J. Makela, B.J. Harding, T.J. Immel (2017), Michelson interferometer for global high-resolution thermospheric imaging (MIGHTI): instrument design and calibration. Space Sci. Rev. doi: 10.1007/s11214-017-0358-4

Ern, M., Preusse, P., Gille, J. C., Hepplewhite, C. L., Mlynczak, M. G., Russell, J. M., and Riese, M. (2011), Implications for atmospheric dynamics derived from global observations of gravity wave momentum flux in stratosphere and mesosphere, J. Geophys. Res., 116, D19107, doi:10.1029/2011JD015821.

Forbes, J. M., Bruinsma, S. L., Doornbos, E., and Zhang, X. (2016), Gravity wave-induced variability of the middle thermosphere, J. Geophys. Res. Space Physics, 121, 6914– 6923, doi:10.1002/2016JA022923.

Fritts, D. C., and M. J. Alexander (2003), Gravity wave dynamics and effects in the middle atmosphere, Rev. Geophys., 41(1), 1003, doi:10.1029/2001RG000106.

Garcia, R. R., T. J. Dunkerton, R. S. Lieberman, and R. A. Vincent (1997), Climatology of the semiannual oscillation of the tropical middle atmosphere. J. Geophys. Res., 102, 26 019–26 032, doi:10.1029/97JD00207.

Harding, B.J., Makela, J.J., Englert, C.R., Marr, K.D., Harlander, J.M., England, S.L. and Immel, T.J. (2017) The MIGHTI Wind Retrieval Algorithm: Description and Verification. Space Science Reviews, 212(1-2), pp.585–600, DOI: 10.1007/s11214-017-0359-3

Harding, B.J., Chau, J.L., He, M., Englert, C.R., Harlander, J.M., Marr, K.D., et al. (2021). Validation of ICON-MIGHTI thermospheric wind observations: 2. Green-line comparisons to specular meteor radars, Journal of Geophysical Research: Space Physics, 126, e2020JA028947, https://doi.org/10.1029/2020JA028947

Harlander, J.M., Englert, C.R., Brown, C.M., Marr, K.D., Miller, I.J., Zastera, V., Bach, B.W. and Mende, S.B. (2017) Michelson interferometer for global high-resolution thermospheric imaging (MIGHTI): monolithic interferometer design and test. Space Science Reviews, 212(1-2), DOI: 10.1007/s11214-017-0374-4

Huffman, G. J. and co-authors (1997), The Global Precipitation Climatology Project (GPCP) combined data set. Bull. Amer. Meteor. Soc., 78, 5-20.

Immel, T.J., England, S.L., Mende, S.B., Heelis, R.A., Englert, C.R., Edelstein, J., Frey, H.U., Taylor, E.R., Craig, W.W., Harris, S.E., Bester, M., Bust, G.S., Crowley, G., Forbes, J.M., Gérard, J.-C., Harlander, J.M., Huba, J.D., Hubert, B., Kamalabadi, F., Makela, J.J., Maute, A.I., Meier, R.R., Raftery, C., Rochus, P., Siegmund, O.H.W., Stephan, A.W., Swenson, G.R., Frey, S., Hysell, D.L., Saito, A., Rider, K.A., and Sirk, M.M. (2018) The Ionospheric Connection Explorer mission: mission goals and design. Space Science Reviews, 214:13 (36pp.). DOI: 10.1007/s11214-017-0449-2.

Liu, H.-L. and S. L. Vadas (2013), Large-scale ionospheric disturbances due to the dissipation of convectively-generated gravity waves over Brazil, J. Geophys. Res, 118, 2419–2427, doi:10.1002/jgra.50244.

Liu, H., N. Pedatella, and K. Hocke (2017), Medium-scale gravity wave activity in the bottomside *F* region in tropical regions, *Geophys. Res. Lett.*, *44*, 7099–7105, doi:10.1002/2017GL073855

Makela, J.J., Baughman, M., Navarro, L.A., Harding, B.J., Englert, C.R., Harlander, J.M., et al. (2021), Validation of ICON-MIGHTI thermospheric wind observations: 1. Nighttime Red-line Ground-Based Fabry-Perot Interferometers, Journal of Geophysical Research: Space Physics, 126. doi:10.1029/2020JA028726.

Maute (2022), WACCMX-SD V2, doi: https://doi.org/10.5065/rjgt-g951.

Miyoshi, Y., H. Fujiwara, H. Jin, and H. Shinagawa (2014), A global view of gravity waves in the thermosphere simulated by a general circulation model, J. Geophys. Res. Space Physics, 119, 5807–5820, doi:10.1002/2014JA019848.

Miyoshi, Y., Fujiwara, H., Jin, H., and Shinagawa, H. (2015), Impacts of sudden stratospheric warming on general circulation of the thermosphere, J. Geophys. Res. Space Physics, 120, 10,897– 10,912, doi:10.1002/2015JA021894.

Preusse, P., S. D. Eckermann, M. Ern, J. Oberheide, R. H. Picard, R. G. Roble, M. Riese, J. M. Russell III, and M. G. Mlynczak (2009), Global ray tracing simulations of the saber gravity wave climatology, J. Geophys. Res., 114(D8):D08126.

Smith, A. K., Pedatella, N. M., Marsh, D. R., & Matsuo, T. (2017). On the Dynamical Control of the Mesosphere–Lower Thermosphere by the Lower and Middle Atmosphere, Journal of the Atmospheric Sciences, 74(3), 933-947. Retrieved Nov 5, 2021, from https://journals.ametsoc.org/view/journals/atsc/74/3/jas-d-16-0226.1.xml

Smith, A. K., Garcia, R. R., Moss, A. C., & Mitchell, N. J. (2017). The Semiannual Oscillation of the Tropical Zonal Wind in the Middle Atmosphere Derived from Satellite Geopotential Height Retrievals, Journal of the Atmospheric Sciences, 74(8), 2413-2425. Retrieved Apr 30, 2022, from https://journals.ametsoc.org/view/journals/atsc/74/8/jas-d-17-0067.1.xml

Stevens, M.H., Englert, C.R., Harlander, J.M., England, S.L., Marr, K.D., Brown, C.M., and Immel, T.J. (2018), Retrieval of Lower Thermospheric Temperatures from O2 A Band Emission: The MIGHTI Experiment on ICON. Space Science Reviews, 214:4 (9pp.). Public access. DOI: 10.1007/s11214-017-0434-9

Vadas SL, Liu H. L. (2013), Numerical modeling of the large-scale neutral and plasma responses to the body forces created by the dissipation of gravity waves from 6 h of deep convection in Brazil, J Geophys Res Space Phys;118:2593–2617. doi: 10.1002/jgra.50249.

Vadas, S. L. and Han-Li Liu (2009), The Generation of Large-Scale Gravity Waves and Neutral Winds in the Thermosphere From the Dissipation of Convectively-Generated Gravity Waves, JGR, 114, A10310, doi:10.1029/2009JA014108.

Vadas, S. L. (2013), Compressiblef-plane solutions to body forces, heatings, and coolings, and application to theprimary and secondary gravity waves generated by a deep convective plume,J. Geophys. Res. Space Physics,118, 2377–2397,doi:10.1002/jgra.50163

Yamashita, C., S. L. England, T. J. Immel, and L. C. Chang (2013), Gravity wave variations during elevated stratopause events using SABER observations, J. Geophys. Res. Atmos., 118, 5287–5303, doi:10.1002/jgrd.50474.

Yiğit, E., A. D. Aylward, and A. S. Medvedev (2008), Parameterization of the effects of vertically propagating gravity waves for thermosphere general circulation models: Sensitivity study, J. Geophys. Res., 113, D19106, doi:10.1029/2008JD010135.

Yiğit, E., A. S. Medvedev (2017), Influence of parameterized small-scale gravity waves on the migrating diurnal tide in Earth's thermosphere, Journal of Geophysical Research: Space Physics, 10.1002/2017JA024089, 122, 4, (4846-4864).

Yiğit, E., and A. S. Medvedev (2012), Parameterization of the effects of vertically propagating gravity waves for thermosphere general circulation models: Sensitivity study. Geophys. Res. Lett., 39, L21101, 10.1029/2012GL053812.

Yiğit, E., A. S. Medvedev, A. D. Aylward, P. Hartogh, and M. J. Harris (2009), Modeling the effects of gravity wave momentum deposition on the general circulation above the turbopause, J. Geophys. Res., 114, D07101, doi:10.1029/2008JD011132.

Yiğit, E. (2017), Dynamics of the Atmosphere-Ionosphere System, Atmospheric and Space Sciences: Ionospheres and Plasma Environments, 10.1007/978-3-319-62006-0_5, (103-133) (2017).

Yuan, T., Stevens, M. H., Englert, C. R., & Immel, T. J. (2021), Temperature tides across the mid-latitude summer turbopause measured by a sodium lidar and MIGHTI/ICON. Journal of

Geophysical Research: Atmospheres, 126, e2021JD035321. Public access. DOI: 10.1029/2021JD035321